

Neutron Detection with High Bandwidth and High Dynamic Range

Jiaping Cheryl Liu

Pittsford Sutherland High School
Pittsford, NY

Advisor: Dr. James P. Knauer

Laboratory for Laser Energetics
University of Rochester
Rochester, NY

November 2009

Abstract

A neutron diagnostic for inertial confinement fusion (ICF) experiments was designed and fabricated that is suitable for both the OMEGA and National Ignition Facility (NIF) laser systems. The diagnostic measures the spectrum of fusion neutrons that are generated at peak compression. The neutrons are downshifted, or lose energy, as they escape depending on the areal density (ρr) of the imploded target. A greater number of downshifted neutrons indicates a greater ρr , a measure of the success of an ICF implosion. The neutrons are detected by transferring energy to charged particles. The neutron detector uses a foil of polyethylene as a source of protons with which neutrons can exchange energy by elastic collisions. The detector also utilizes tungsten as a shield for x-ray radiation emitted from the target. The neutron detector exhibits high bandwidth and an exceptional dynamic range of 10^{10} which is ideal for measuring neutron spectra from implosion and ignition experiments. The detector will be tested with protons from the Multi-Terawatt laser, tested with neutrons from OMEGA, and ultimately used to diagnose NIF implosion and ignition experiments.

1. Introduction

Inertial confinement fusion (ICF) is a process where nuclear fusion reactions are initiated by rapidly heating and compressing a target, typically in the form of a pellet that consists of a thin plastic external layer and an internal mixture of the hydrogen isotopes deuterium and tritium. ICF implosions create the possibility of cleaner, limitless, and more cost effective energy. For fusion power to be considered practical, a state of ignition must be achieved. Ignition refers to the point at which the energy given off in the fusion reactions is high enough to cause fusion reactions in the surrounding fuel. This causes a chain reaction that allows the

majority of the fuel to undergo a nuclear “burn” and produces more output energy than the energy consumed by the laser. Currently, lasers consume more energy than they produce during implosions and thus for an implosion to be considered successful the energy produced must be much higher than the laser energy. The OMEGA laser at the University of Rochester has 60 laser beams that focus up to 30 kJ of energy onto targets. Although very powerful, it cannot obtain ignition. The Lawrence Livermore National Laboratory’s National Ignition Facility (NIF) is a new 1.8 MJ, 192-laser-beam system designed to achieve nuclear fusion ignition completed in 2009.¹ The NIF replaced the OMEGA laser facility as the most powerful laser system in the world.

In ICF experiments, primary energetic neutrons are produced by two reactions:



Neutrons generated from deuterium-deuterium reactions have energies of 2.45 MeV while neutrons generated from deuterium-tritium reactions have higher energies of 14.1 MeV.

The fusion neutrons travel through the relatively “cold” fuel shell of the target and some are scattered. The neutrons are down-scattered or downshifted, meaning that they lose energy as they escape. Some neutrons will scatter more than others, creating a spectrum of the downshifted neutrons. The downscattered neutrons are generated when the areal density (ρr), the density ρ of the cold fuel shell times its thickness r , is high. A high areal density is important for the success of an implosion because the chain reaction of ignition requires compression of a sufficient thickness of fuel (ρr). Typically, DT fuel is used as the inner fuel of the target. Sufficient ρr is necessary for chain reactions to occur because alpha particles traveling through the compressed fuel deposit their energy only when the ρr is high enough. Neutron diagnostics

that measure the neutron spectra therefore enable the ρr to be measured, providing valuable information on the success of implosion and ignition experiments.

This work exhibits the design and fabrication of a new neutron “diode” which will be able to measure full neutron spectra with a much higher bandwidth and dynamic range than existing detectors. Figure I gives a schematic of the design concept of the neutron diode and the correspondence of the neutron spectrum to the recorded signal of the detector.

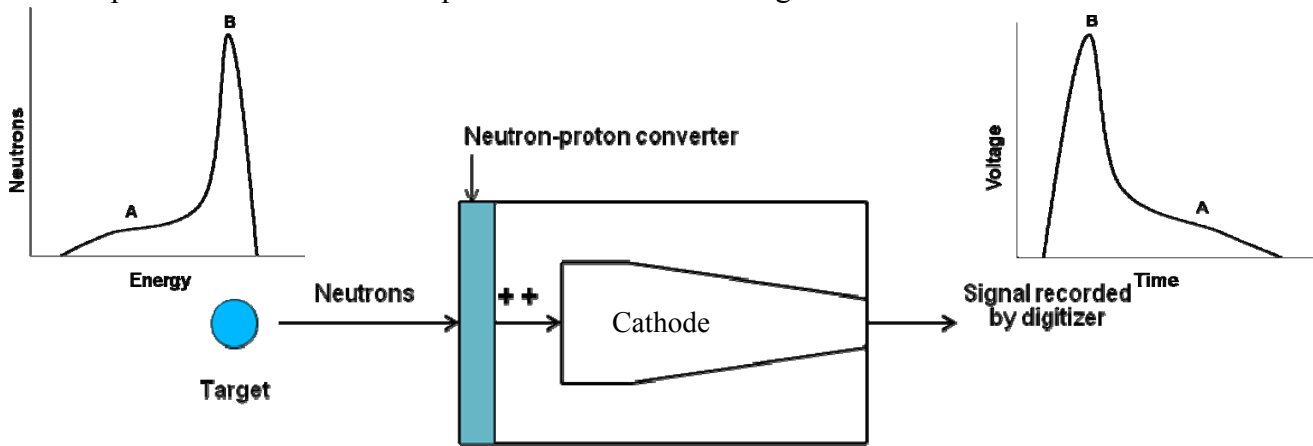


FIG. I. Design concept for neutron diode in target chamber

Incoming neutrons encounter a plastic converter foil where they transfer energy to protons. Energy transfers within the diode from neutrons to charged particles are crucial for detecting neutrons because neutrons are electrically neutral particles and thus do not respond to electric fields. The neutrons can transfer almost all of their kinetic energies to protons during direct, elastic collisions because of the similarity in their masses. A proton flux exits the plastic neutron-proton converter and attracts towards the negatively charged cathode. Secondary electrons are emitted from proton bombardment upon the cathode. Together the electrons and protons produce an electrical current and a signal voltage across a 50 Ω impedance that is recorded by a digitizer. Figure I shows the concept that neutrons of higher energy arrive at the diode first and thus the signals from higher energy neutrons are recorded first.

Prior to this work, the concept of this diode has not been used in neutron detectors because of the low neutron-proton cross section. However, this detector is feasible because of the large neutron yield expected from the National Ignition Facility. In this work, a neutron detector was designed and fabricated. The detector exhibits higher bandwidth and higher dynamic range than existing neutron detectors. Simulations of expected signals have been made for the Multi-Terawatt (MTW), OMEGA, and NIF laser systems. The neutron diode will first be tested with protons from the MTW laser, a high intensity laser at the Laboratory for Laser Energetics. The diode will then be used to diagnose implosions on the OMEGA system. Ultimately, it will be used to diagnose ignition experiments on the NIF.

2. Design of the detector

2.1 Design concept

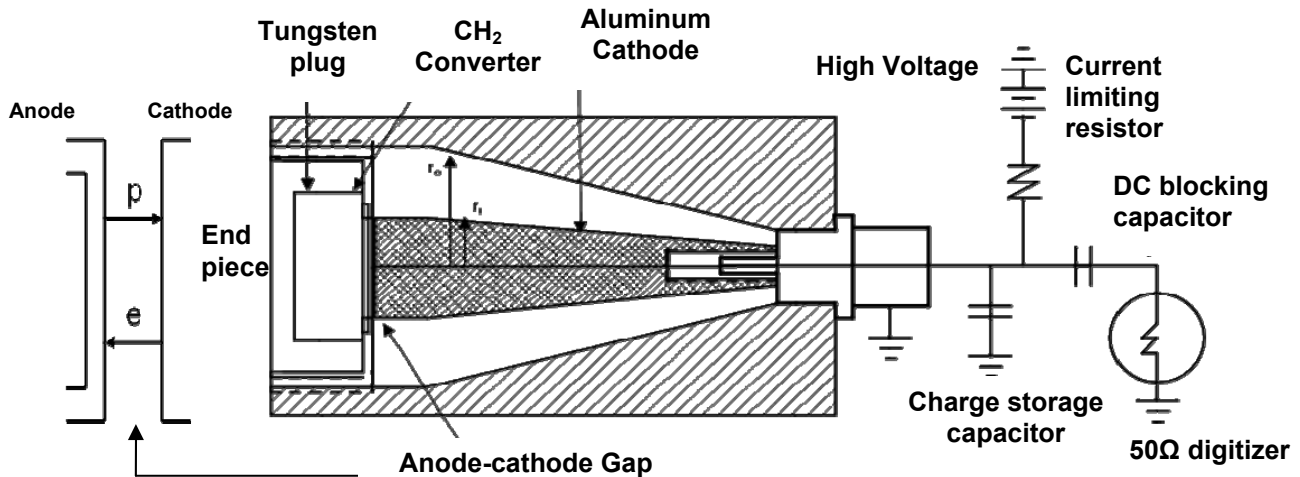


FIG. II. Detailed drawing of neutron diode and anode-cathode gap

Figure II shows a detailed drawing of the neutron diode and with a zoom on the anode-cathode gap. The main parts include a cathode, a washer which serves as the anode, an end piece holding a tungsten plug to close the detector and block unwanted radiation, a plastic (CH₂) neutron-proton converter, a set screw to attach the connector, and a main housing compartment

to lodge and protect all the above parts. The gap between the anode and the cathode creates an electric field with protons flowing towards the cathode and electrons toward the anode, or the washer. The current limiting resistor prevents the current from reaching the high voltage. High voltage is applied through a commercially available² bias tee. The DC blocking capacitor ensures that the high voltage does not go across the 50 Ω digitizer. The charge storage capacitor helps maintain the voltage across the cathode-anode gap between the CH₂ foil and cathode. The signal is recorded by the 50 Ω digitizer.

The neutron-proton scattering cross section is crucial for calculating the number of protons expected to reach the cathode. Table I shows a comparison of calculated and experimental values for the neutron-proton cross section for 14 MeV neutrons.

TABLE I. Summary of calculated and experimental n-p cross sections

Type of data	Energy (MeV)	Cross Section (barns)	Reference
Calculated	14	0.694 ± .019	Agno ³
Calculated	14	0.69	Sleator ⁴
Calculated	14	0.6929	Bame, Haddad, Perry ⁵
Calculated	14	0.70 ± 0.06	Salant and Ramsey ⁶
Calculated	14.10	0.689 ± 0.005	Poss, Salant, and Yuan ⁷
Experimental	14.10	0.688	Poss, Salant, and Yuan ⁷
Experimental	14.12	0.687	Coon, Graves, and Barschall ⁸
Calculated	14.20	0.675 ± 0.02	Meyer and Nyer ⁹

From these data, the average neutron-proton cross section is 0.69 barns or $6.9 \times 10^{-25} \text{ cm}^2$ for 14.1 MeV neutrons. The neutron-proton section is $2 \times 10^{-24} \text{ cm}^2$ for 2.523 MeV neutrons.¹⁰

The quantum efficiency of protons to electrons is also required. Figure III shows the yields of secondary electrons per primary proton for aluminum.

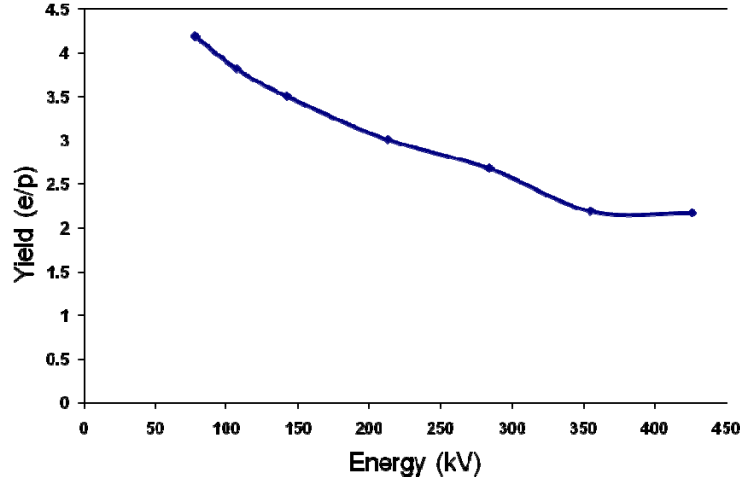


FIG. III. Yield of secondary electrons per primary proton on an aluminum target. Experimental yield obtained by Hill et al.¹¹

Based on Figure III, the quantum efficiency can be assumed to be two electrons per proton for protons with energies above 400 kV.^{11,12}

The expected signal can be calculated through a series of steps. The number of neutrons (N_n) reaching the converter is given by:

$$N_n = Y \cdot (A_d / 4\pi d^2) \tag{3}$$

where Y is the neutron yield, d is the distance from the target and A_d is the area of the cathode of the detector.

The number of protons (N_p) produced in the converter can be calculated by:

$$N_p = N_n \cdot \tau \cdot \sigma \cdot r \tag{4}$$

where τ is the proton-neutron cross section, σ is the number of protons per cm^3 in the converter and r is the depth of the converter. Low density polyethylene (LDPE), the converter used for the neutron diode, has a density of 0.92 g/cm^3 , a molecular weight of approximately 14 g/mol and two protons per molecule, giving $\sigma = 8 \times 10^{22} \text{ protons/cm}^3$. Low density polyethylene was chosen because of its large proton density as shown in Table II and because it is more readily available than high density polyethylene (HDPE).

TABLE II. Comparison of proton densities of different materials

Material	Density of Material (g/cm ³)	Proton density (protons/cm ³)
CH	1.02	4.72 x 10 ²²
CH ₂ (LDPE)	0.92	7.92 x 10 ²²
CH ₂ (HDPE)	0.95	8.17 x 10 ²²
H ₂ O	1.00	6.69 x 10 ²²

The neutron diode is designed to measure the neutron spectrum from 9 to 15 MeV with 5% accuracy. To achieve this, the neutron detector requires a high enough dynamic range. The dynamic range of the neutron detector is defined as

$$DR_{\max} = V_{\max} / V_{\min} \tag{5}$$

where V_{\max} is the maximum detectable voltage and V_{\min} is the minimum detectable voltage. If the maximum and minimum signal voltages are S_{\max} and S_{\min} , respectively, and are to be measured with a precision ϵ , it is required that

$$DR_{\max} = S_{\max} / S_{\min} \cdot (1 / \epsilon)^2 \tag{6}$$

Using $\epsilon = 0.05$, this will require a detector with a dynamic range of at least 4.0×10^6 if the signal ratio S_{\max} / S_{\min} is 10^4 .

Scintillators and chemical vapor deposition (CVD) diamond detectors typically have a dynamic range of 4×10^4 to 4×10^6 . These detectors are useful for measuring the neutron spectrum for implosion experiments with lower neutron yields and detecting single neutrons; however they cannot fully measure neutron spectra for implosion experiments of higher peak yields, such as ignition reactions. Because the neutron diode has a minimum output voltage of 0.1 μ V and a maximum output voltage of 1.2 kV, the diode has an estimated dynamic range

(DR_{\max}) of 10^{10} and thus is able to measure the full neutron spectrum for the higher peak yields of break-even and ignition campaign experiments.

2.2. Detailed design

The neutron diode was designed using Ashlar Vellum’s *Graphite*¹³ computer aided design program. Figure IV shows the key parts of the fabricated diode. The design process and individual pieces of the neutron diode are detailed in this section.



FIG. IV. Parts of the detector unassembled. Labeled are the key parts of the detector. (1) Housing (2) Threaded washer (3) Polyethylene converter (4) Tungsten plug (5) End piece (6) Cathode

For the detector to avoid unwanted reflected signals while measuring the signal, maintaining uniform impedance is crucial. A large surface area of the cathode is desired so that a higher number of protons will hit it and produce a larger signal. Thus, the cathode is tapered so the frontal surface has a large surface area and the rear is fitted to the smaller connector. However, because the cathode is tapered the inside of the housing is also tapered to maintain uniform impedance (Z) throughout the detector. Equation (7)¹⁴ is used:

$$Z = 60 \ln (r_o/r_i) \Omega \quad (7)$$

where r_o is the outer radius and r_i is the inner radius which are labeled on Figure II. An impedance of 50Ω was chosen to match the recorder input impedance. Choosing 10 mm for r_i or the inner radius of the housing compartment at the converter end of the detector, 23 mm is obtained for the outer radius, r_o . By choosing a r_i of 4 mm at the connector end of the cathode, a r_o of 9.2 mm must be used.

To accommodate the electrical connection to the detector, a type N connector was chosen because of the need to bias the cathode with a high voltage. To fit this connector, a tapped 8.4 mm space was set in the back of the detector. In order to easily attach the cathode and the connector to the main housing, the cathode was drilled and tapped for a $\frac{1}{4}$ ”-28 thread so that a set screw can be screwed into the cathode.

The aluminum threaded washer serves to hold both the neutron-proton converter and end piece in place. It is tapped for a 2”-12 thread and a $1 \frac{3}{4}$ ” -12 thread so that the end piece can be screwed onto it and to allow for adjustments within the housing. The washer leaves a 1 mm space in the front for the 1 mm polyethylene converter to fit into.

In order to create an electric field between the washer (anode) and the cathode, a small gap large enough for a proton to travel in 100 picoseconds was included. This gap was calculated to be 0.6 mm, but for the purposes of the detector it was rounded to 0.5 mm.

The aluminum housing features a tapered shape and two threaded openings: one in the front for the end piece and one in the rear of the detector for the connector. Because various gases may enter the detector in the target chamber, two cinkered plugs are placed on opposite sides of the main housing. These allow gases such as air to escape the detector.

The end piece serves a dual function: it closes and protects the detector but more importantly it serves to shield the detector from gamma and x-rays emitted from the target during

implosions. The measure of the effectiveness of the material as a gamma shield is called the “half value thickness,” that is, the thickness of a material that will reduce the gamma ray exposure by 50 percent. To maximize the absorption of gamma and x-ray radiation from the imploded target, a substance with a very low half thickness is desired. Tungsten has one of the lowest half value thicknesses of 0.04 cm, and unlike other substances with very low half value thicknesses such as uranium, it does not emit excess radiation through decay and thus does not create excessive, unwanted background signal. Also, while tungsten absorbs x-ray radiation, it will not absorb or shield any neutrons. Because of tungsten’s low half value thickness, a 13 mm tungsten plug is employed as part of the end piece.

Aluminum was chosen as the material for a majority of the parts, because aluminum, unlike other metals such as stainless steel, does not react or become activated during implosion experiments and thus does not create unwanted background signals.

3. Comparison with other neutron detectors

There are several types of detectors that are currently used for neutron detection. The most popular and effective are scintillators and chemical vapor deposition (CVD) fabricated diamond detectors.

Table III gives a comparison of several existing neutron diagnostics with the new neutron diode. All data for the neutron diode are calculated values while values for other types are experimental or commercially available.^{15,16} It is evident that the new neutron diode displays much higher bandwidth (shorter rise and decay times) than both scintillator and CVD diamond detectors as well as an exceptionally large dynamic range in comparison to existing neutron

diagnostics. In addition to high dynamic range and bandwidth, the neutron diode is shielded for x-ray radiation and it is less sensitive to gamma radiation because of the tungsten shielding.

TABLE III. Comparison of the bandwidth and dynamic range of the new neutron diode with other types of detectors

Type of detector	Rise time	Decay time	Dynamic Range
Nonplastic Scintillator ¹⁵	250 ns	Up to 2 ms	10 ⁴
Plastic Scintillator ¹⁵	<1 ns	2-3 ns	10 ⁵
Liquid Scintillator ¹⁵	<1 ns	<1 ns	10 ⁴
CVD diamond detector ¹⁶	200 ps	5 ns	10 ⁴
Neutron diode	46 ps	275 ps	10 ¹⁰

4. Results

Calculations of expected signals have been developed for the Multi-Terawatt (MTW) laser system, the OMEGA laser system, and the new National Ignition Facility (NIF) .

4.1 Predicted signals for the Multi-Terawatt laser

The Multi-Terawatt laser system emits protons and gamma rays in laser-solid interactions when targets are irradiated with short pulse lasers. Protons originate from layers of contamination on the target surfaces. MTW is suitable for testing the new neutron diode because of its proton emission. The CH₂ converter will be unnecessary for these tests and will be taken out from the washer because the diode will directly detect protons.

Calculations have been made to ensure that the protons emitted will be able to override the gamma radiation that is also emitted based on previous target shots. To further attenuate the background photon signal, a 0.01 cm aluminum transmission filter will be placed in the space in

the washer in place of the CH₂ converter. The filter will attenuate photons with energies less than 7000 eV.

To estimate the signal from protons, the expected proton spectrum on MTW is necessary. This has not been previously measured. However, Kaluza et al.¹⁷ present a proton spectrum from a laser system similar to MTW for targets of different thickness aluminum foils (see Fig. V). Figure V gives $dN_p/(dE \cdot d\Omega)$, the number of protons in energy interval dE and solid angle $d\Omega$ as a function of proton energy E .

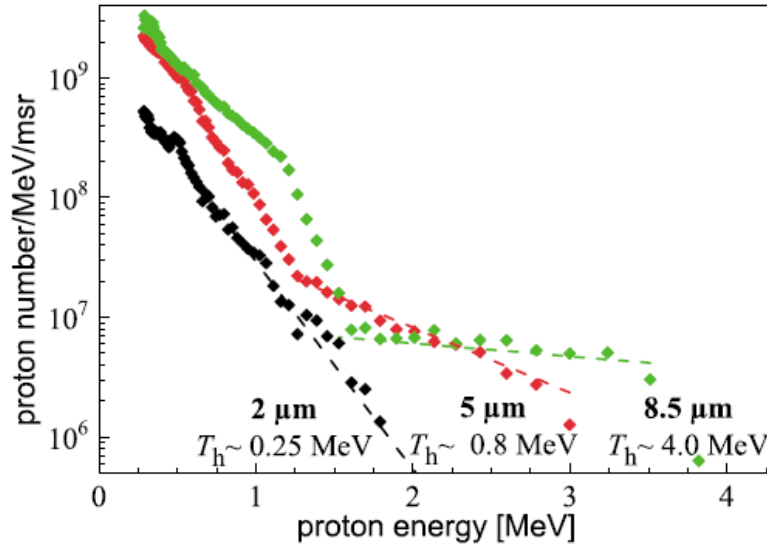


FIG. V. Proton spectra from aluminum foils of varying thickness

The signal received by the detector depends on the rate of arrival of protons at the detector dN_p/dt and is calculated as follows:

$$dN_p/dt = dN_p/dE \cdot dE/dt \quad (8)$$

$$dN_p/dE = dN_p/(dE \cdot d\Omega) \cdot \Delta\Omega \quad (9)$$

$$\Delta\Omega = A_d/d^2 \quad (10)$$

where dN_p/dE is the number of protons as a function of proton energy, dE/dt is the proton energy as a function of time, $\Delta\Omega$ is the solid angle of the detector, A_d is the area of the frontal

surface of the cathode and d is the distance from the target chamber center that the detector will be placed. Since $E = \frac{1}{2} m (d/t)^2$, dE/dt is given by

$$dE/dt = (1/d\sqrt{m}) \cdot 2E^{3/2} \tag{11}$$

The number of electrons as a function of time is given by

$$dN_e/dt = dN_p/dt \cdot QE \tag{12}$$

where QE is the quantum efficiency. The current can then be calculated:

$$I = (dN_e/dt + dN_p/dt) \cdot q_e \tag{13}$$

where q_e is the charge of an electron. Using Ohm’s law with a 50Ω resistance will yield the voltage signal. Figure VI shows the expected signals from the protons from aluminum targets when the detector is placed 90 cm away from the target chamber center. Higher voltages are expected at later times because more protons of lower energies arrive at later times. This is different from the case of fusion neutrons where a small number of neutrons come at later times, but applying the neutron diode in MTW serves to test the diode.

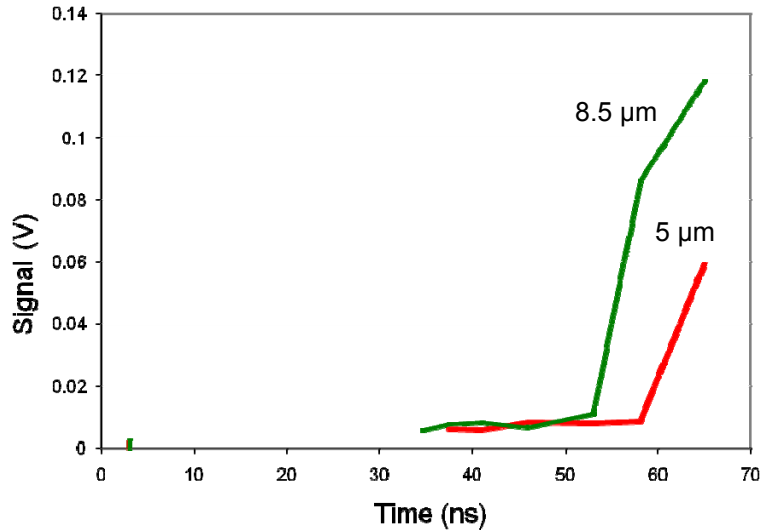


FIG. VI. Calculated signals from protons on the MTW laser as a function of time, based on the spectra of FIG. V for 8.5 and 5 μm aluminum targets.

4.2 Predicted signals for OMEGA

OMEGA implosions typically have neutron yields (Y) in the range of 10^9 to 10^{14} . Figure VII shows the predicted neutron spectra from two typical OMEGA implosion experiments¹⁸ with areal densities (ρr) of 100 and 200 mg/cm². The two ρr curves show that an increased ρr corresponds to more downscattered neutrons. Thus ratios of the number of downscattered neutrons can determine the ρr , a measure of the success of the implosion. These calculations show that as the ρr doubles, the number of neutrons/MeV doubles. The graph is shown in terms of the number of neutrons/total DT neutron yield/MeV.

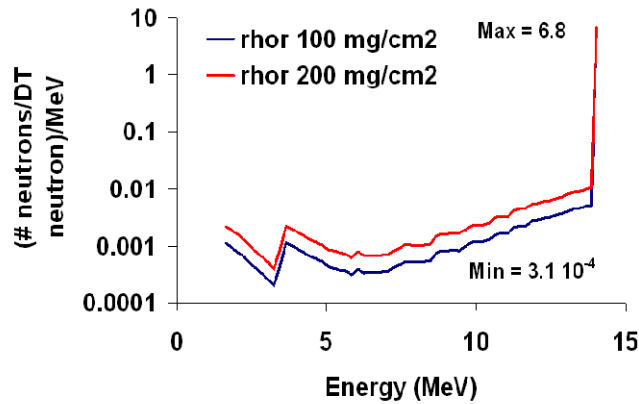


FIG. VII. DT Neutron spectrum from an OMEGA implosion experiment

Using Equations (8) through (13) with N_p replaced by N_n and the neutron-proton cross sections, the expected signals have been calculated and are shown in Figure VIII with an estimated total neutron yield of 10^{10} . Placing the detector a distance of 40 cm away from the target chamber center on OMEGA, a reasonable maximum signal of 0.19 volts with a ρr of 200 mg/cm² is obtained which is well in within the detectable signal range. The signal peaks at 7.69 ns as a result of the 14.1 MeV DT neutrons. The diode will be able to detect neutrons for implosions yielding up to 10^{13} at a distance of 40 cm away from the target chamber center because of the large dynamic range.

The minimum signal ($4 \mu\text{V}$) is above the minimum output voltage ($0.1 \mu\text{V}$), and so the neutron diode should be easily capable of measuring the neutron spectra for future implosion experiments on OMEGA.

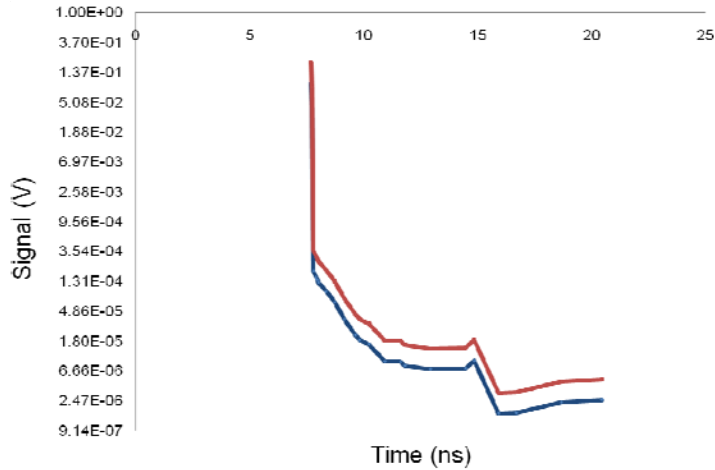


Fig VIII. Expected signal from OMEGA with a neutron yield of 10^{10} , showing the downscattered neutrons for two values of areal density, ρr . The blue curve corresponds to a ρr of 100 mg/cm^2 while the curve in red corresponds to a ρr of 200 mg/cm^2 .

4.3 Predicted signals for the National Ignition Facility

Figure IX shows simulated neutron spectra for the tritium hydrogen deuterium (THD) campaign on the NIF laser system.¹⁸ The THD campaign uses targets filled with mostly tritium to produce implosions that are hydrodynamically equivalent but produce a reduced number of neutrons. Thus the campaign is a plan for testing and perfecting the target fuel content and target chamber conditions to be done on the NIF to ensure all conditions are ideal before attempting real ignition experiments. In colors are spectra from targets with 0.5% D_2 fuel that are not meant to ignite and serve as tests for the NIF. In black is a spectrum with 50% D_2 fuel that was calculated without alpha particle deposition to serve as model for a non-igniting target. The ρr is determined by the region of 9 MeV to 15 MeV neutrons.

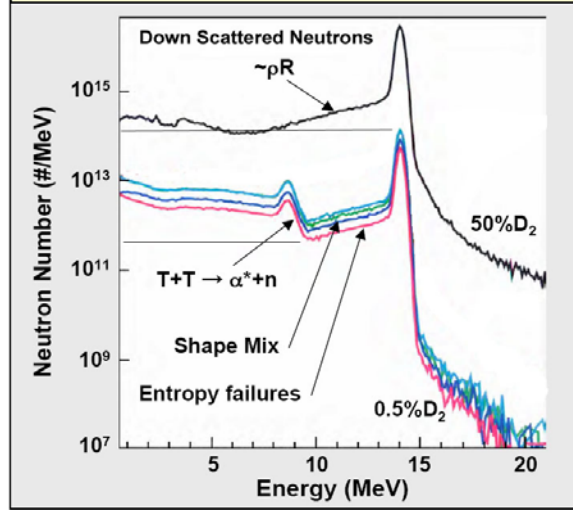


FIG. IX. Simulated neutron spectra for NIF for 50:50 DT (black curve) and for THD targets containing 0.5% D₂ (colors)

The typical neutron yield on the NIF ranges from 10^{13} to 10^{18} . For initial experiments with lower neutron yields, the detector can be placed 40 cm away from the target chamber center like the experiments using OMEGA. For 50% D₂ experiments with higher neutron yields, it will be necessary to move the detector farther away to 400 cm from the target chamber center so the signal is within the dynamic range of the detector.

Figure X(a) shows the expected signal on the NIF when the neutron diode is placed 400 cm from the target chamber center (TCC) for ignition campaign experiments using targets of 50% D₂ fuel while Figure X(b) shows that of targets using 0.5% D₂ fuel placed 40 cm away from the target chamber center. Figure X(a) peaks at 77.2 ns with a voltage of 233.3 V and Figure X(b) peaks at 7.72 ns with a voltage of 6.67 V. The discrepancy between the times is due to the different distances between the diode and the center of the target chamber. Both signals are within the detectable range of the neutron diode and thus the diode can be used effectively on the National Ignition Facility.

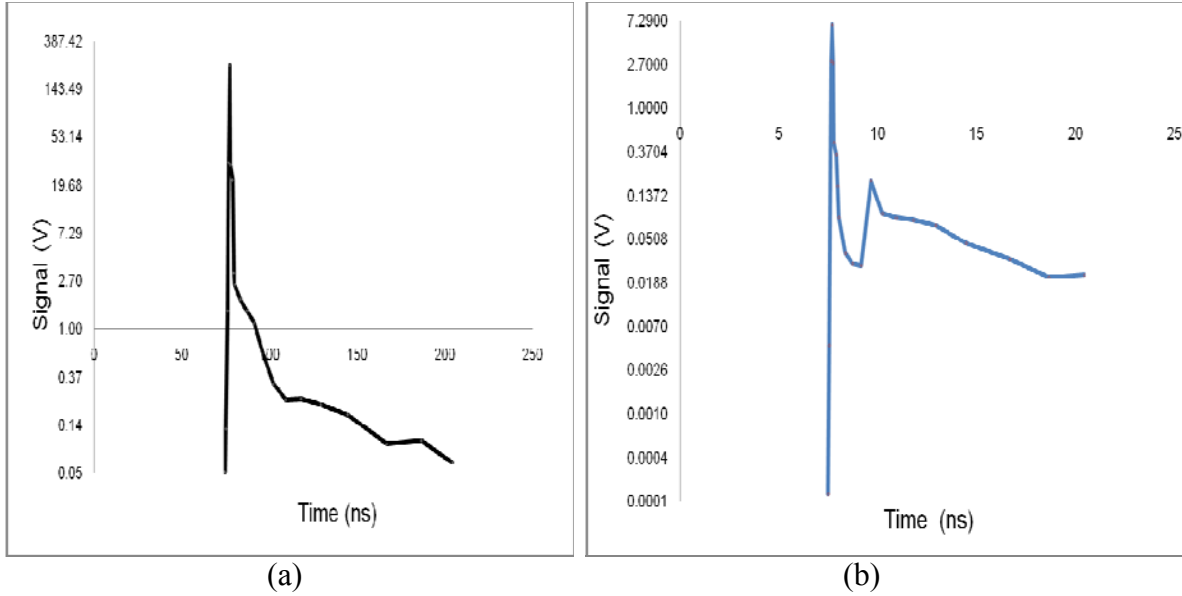


FIG. X. Expected signals on the NIF corresponding to
 (a) 50% D_2 curve with detector placed 400 cm from TCC (black)
 (b) 0.5% D_2 curve with detector placed 40 cm from TCC (blue)

Conclusion:

A neutron detector with high bandwidth and dynamic range was designed and fabricated. Expected signals were calculated for the MTW, OMEGA, and NIF laser systems. These signals are all within the dynamic range of the detector with the detector placed 90 cm away from the target chamber center for MTW, 40 cm away for OMEGA and 400 cm during THD ignition campaign experiments of the NIF.

It has been demonstrated from the predicted signals that the detector is useful not only for the MTW and OMEGA laser facilities but also for the new laser facility at the NIF. The next step is to test the neutron diode on MTW, using protons to simulate results on OMEGA and the NIF. From there, the diode can be further used to diagnose OMEGA experiments and eventually ICF ignition campaign experiments on the NIF.

The diode presented in this work is significant because it has an exceptional dynamic range that will enable it to measure the full neutron spectra of implosion and ignition campaign

experiments. On the National Ignition Facility, the detector will be used to measure the success of THD ignition campaign experiments, helping to bring fusion experiments closer to providing a source of clean, limitless energy.

Acknowledgements:

I would like to thank my advisor, Dr. James P. Knauer for his immense support, advice, and patience. I would also like to thank Dr. R. S. Craxton, the University of Rochester’s Laboratory for Laser Energetics and the United States Department of Energy for providing me the opportunity to participate in this inspiring program.

References:

1. E. I. Moses, *Fusion Sci Technol.* **44**, 11 (2003).
2. Picosecond Pulse Labs, Inc. (http://www.picosecond.com/product/product.asp?prod_id=90)
3. Ageno *et al.*, *Phys. Rev.* **71**, 20 (1947).
4. W. Sleator, *Phys. Rev.* **72**, 207 (1947).
5. S. J. Bame, *et al.*, *Rev. Sci. Instrum.* **28**, 12 (1957).
6. E. O. Salant and N. F. Ramsey, *Phys. Rev.* **57**, 1075 (1940).
7. H. Poss, *et al.*, *Phys. Rev.* **87**, 11 (1952).
8. Coon *et al.*, *Phys. Rev.* **88**, 562 (1952).
9. D. I. Meyer and W. Nyer, Los Alamos Report No. 1279 (1951).
10. Fields, *et al.*, *Phys. Rev.* **94**, 389 (1954).
11. A. G. Hill, *et al.*, *Phys. Rev.* **55**, 463 (1939).
12. S. Bartholome, *et al.*, *Nucl. Instrum. And Meth. In Phys. Res. B* **125**, 13 (1997).

13. *Graphite*, Ashlar-Vellum, Inc., 9600 Great Hills Trail, Suite 150W-1625, Austin, TX 78759, 2001.
14. D. Gray, *American Institute of Physics Handbook*, 3rd ed. (McGraw-Hill, New York, 1972), p. 5-57.
15. Amcrys-H, Inc., 60 Lenin Ave, Kharkov 310001, Ukraine, 1998.
16. G. J. Schmid, *et al.*, *Rev. Sci. Instrum.* **74**, 1828 (2003).
17. M. Kaluza, *et al.*, *Phys. Rev. Lett.* **94**, 045003 (2004).
18. J. P. Knauer, private communication (2009).